PROCEEDINGS B

royalsocietypublishing.org/journal/rspb

Research

Cite this article: Khandelwal PC, Hedrick TL. 2020 How biomechanics, path planning and sensing enable gliding flight in a natural environment. *Proc. R. Soc. B* **287**: 20192888.
http://dx.doi.org/10.1098/rspb.2019.2888

Received: 12 December 2019
Accepted: 23 January 2020

Subject Category:
Morphology and biomechanics

Subject Areas:
biomechanics, behaviour, ecology

Keywords:
Draco, guidance, obstacle-avoidance, collision-free flight

Author for correspondence:
Tyson L. Hedrick
e-mail: thedrick@bio.unc.edu

Electronic supplementary material is available online at https://doi.org/10.6084/m9.figshare.c.4835253.

THE ROYAL SOCIETY PUBLISHING

How biomechanics, path planning and sensing enable gliding flight in a natural environment

Pranav C. Khandelwal and Tyson L. Hedrick

Department of Biology, University of North Carolina at Chapel Hill, Chapel Hill, NC, USA

PCK, 0000-0002-0589-4467; TLH, 0000-0002-6573-9602

Gliding animals traverse cluttered aerial environments when performing ecologically relevant behaviours. However, it is unknown how gliders execute collision-free flight over varying distances to reach their intended target. We quantified complete glide trajectories amid obstacles in a naturally behaving population of gliding lizards inhabiting a rainforest reserve. In this cluttered habitat, the lizards used glide paths with fewer obstacles than alternatives of similar distance. Their takeoff direction oriented them away from obstacles in their path and they subsequently made mid-air turns with accelerations of up to 0.5 g to reorient towards the target tree. These manoeuvres agreed well with a vision-based steering model which maximized their bearing angle with the obstacle while minimizing it with the target tree. Nonetheless, negotiating obstacles reduced mid-glide shallowing rates, implying greater loss of altitude. Finally, the lizards initiated a pitch-up landing manoeuvre consistent with a visual trigger model, suggesting that the landing decision was based on the optical size and speed of the target. They subsequently followed a controlled-collision approach towards the target, ending with variable impact speeds. Overall, the visually guided path planning strategy that enabled collision-free gliding required continuous changes in the gliding kinematics such that the lizards never attained theoretically ideal steady-state glide dynamics.

1. Introduction

Terrestrial habitats are complex spatial structures, frequently traversed by animals to perform behaviours essential for their survival. Different modes of locomotion necessitate that animals use varied biomechanical strategies and sensory inputs to precisely navigate their environment while maintaining physical stability and speed. For example, on land, scrub lizards normally use quadrupedal running but reduce their sprint speed to negotiate obstacles with occasional switches to bipedal running [1]. Cockroaches use a mechanically mediated strategy, taking advantage of their body shape and mechanical feedback from the environment to reorient their body while moving through clutter [2]. Unlike terrestrial locomotion, volant taxa have an added constraint of maintaining minimum lift to stay aloft, either from flapping and/or maintaining forward speed. To manoeuvre, flying birds reduce forward speed and increase flapping frequency to perform turns mid-air [3]. Altogether, such strategies involve generating directional forces, along with propulsive forces, to alter the animal's path to either negotiate an obstacle or reorient towards the desired target. Gliding animals power flight by trading altitude for kinetic energy to ultimately generate lift for locomotion, facing the additional constraint of a finite energy supply for powering manoeuvres. Furthermore, gliding taxa often have simpler wing anatomy with fewer degrees of freedom than flapping flyers such as birds or bats. Despite such limitations, gliders like colugos, squirrels, snakes and lizards thrive in dense forests presenting complex three-dimensional spatial geometries. They frequently glide to forage, seek mates, defend territories and avoid predators [4], behaviours that have direct fitness

consequences. Collision-free flight is key to their survival, yet how animals execute such glides in their natural habitat remains unclear.

Among gliding terrestrial vertebrates, laboratory studies have described the mechanics of parts of the glide in detail, including takeoff and landing in flying squirrels and sugar gliders [5–9]. These studies produced high-resolution kinematic data of the animal but lacked information of the behavioural context and entirety of the glide which might be crucial to understanding the observed outcomes. Additionally, captivity and a laboratory setting might limit or influence the animal's behaviour. Field studies have explored gliding behaviour using animal-borne data loggers in colugos, providing takeoff and landing kinematics [10] and energetic costs of gliding [11]. Field recordings on flying lizards have described simple glide metrics such as glide angle and ratio in two dimensions along with speed and acceleration estimates [12]. Non-equilibrium gliding biomechanics of wild flying squirrels and snakes has been studied while departing from a single takeoff location with limited landing options [13,14]. While data loggers do not capture body shape changes undertaken by the animal or the environmental context, video recordings limit the spatial scale at which gliding can be observed. Furthermore, observational studies on Siberian flying squirrels have shown gliding patterns to be related to the forest structure, capturing the environmental context but lacking kinematic details [15,16]. Thus, the above studies look at specific aspects of the glide, but none offer a holistic view of gliding biomechanics in the animal's natural habitat. We used an ultra-portable three-dimensional stereo videography set-up to study locomotory strategies employed by wild, freely behaving flying lizards (*Draco dussumieri*) traversing a naturally cluttered habitat. This video tracking approach captured the lizard's motion covering the entire takeoff to landing duration along with the environmental features which it might have encountered while gliding. The resulting dataset incorporated the combined effect of behaviour and the environment on the gliding biomechanics of the animal allowing us to address the following hypotheses.

We hypothesized that in a natural environment, flying lizards would use a glide profile including a ballistic descent to gain speed followed by a non-equilibrium mid-glide to cover distance and negotiate obstacles, and finally a swoop-up landing manoeuvre to decelerate and reduce the energy dissipated at impact. Our expectation of non-equilibrium glide kinematics is in contrast to previously reported equilibrium glides in *Draco* between fixed takeoff and landing poles [12], but similar to observations in flying squirrels [4,13]. Next, a cluttered environment may present obstacles that will require flying lizards to execute lateral manoeuvres. Producing such manoeuvres requires either a reduction in upward force or an increase in total lift, both leading to a greater loss of altitude (energy) for a given glide distance. Hence, we hypothesized that lizards would preferentially use a path planning strategy to minimize the energetic losses due to manoeuvring. Alternatively, lizards may simply avoid glides that require them to fly around an obstacle, restricting them to glide distances similar to the average spacing between trees in their habitat. Lastly, we assumed vision to be the primary sensory modality used by *Draco* to navigate their natural habitat. In this case, the spatial uncertainty of environmental features (obstacles and targets) increases with glide distance. Thus, we hypothesized that lizards control their heading direction based on an existing vision-based obstacle-avoidance steering model [17], but may reactively respond to potential obstacles mid-air during longer glides. Furthermore, we assumed that lizards use their optical flow field to derive the distance and approach speed to the landing tree. Therefore, we predicted that they initiate their landing approach based on a critical value of the optical size and speed of the target as described by the relative retinal expansion velocity (RREV) model, as has been previously reported in groups as diverse as fruit flies and birds [18–20].

2. Material and methods

(a) Field site

The field site was a roughly 115 × 60 m abandoned areca nut (*Areca catechu*) plantation located within the Agumbe Rainforest Research Station (ARRS) campus, Karnataka, India (13°31′04″ N, 75°05′18″ E). The site was enclosed by open habitat on the east, and a mix of open habitat and tropical rainforest on the other sides. The site contained approximately 912 areca nut trees (approx. 13 trees per 100 m^2) mixed with scattered local flora. The trees were approximately 10 cm to approximately 20 cm in diameter, approximately 5 m to approximately 23 m tall and had an inter-tree distance of approximately 1.5 m to approximately 8 m, providing areas of varying tree clutter. A population of flying lizards (*D. dussumieri*) inhabited the plantation during the breeding season (February–May). The number of lizards at the field site during data collection was unknown, but a study at this site in 2017 identified 33 individuals (16 males), i.e. approximately 4.7 lizards per 1000 m^2 [21].

(b) Animals

Our study species *D. dussumieri* is a medium-sized flying lizard (max snout–vent length = 9.7 cm [22]), endemic to the Western Ghats region of southern India. They are found inhabiting plantations, secondary, and evergreen forests ranging from 80 to 1300 m elevation above sea level [23]. The lizards are diurnal and use gliding as the main mode of locomotion to traverse among trees in their natural habitat [24]. Unlike other gliding animals, *Draco* glide using a unique primary wing composed of membrane attached to a set of 5–7 elongated ribs on either side [25]. When gliding, the wings are stretched open by rotating the ribs laterally. Secondary force-generating structures include lappets on the lateral margins of the head along with almost planar fore and hind limbs. During the landing phase of the glide, the ribs collapse medially, folding the wings and facilitating movement on trees. Frequent glides can be observed by lizards during the mating season (February–May) as the lizards forage, defend territories (male–male encounters) or seek mates (male–female encounters).

(i) Glide phases

We developed consistent definitions for dividing complete glides into takeoff, mid-glide and landing phases based on characteristic changes in centripetal acceleration and horizontal speed (figure 1*b*).

Takeoff consisted of jumping from the takeoff tree followed by wing deployment. These morphological adjustments resulted in an increase in aerodynamic lift force with lizards transitioning from a mostly downwards to mostly forward motion. During this transition, the resultant aerodynamic force vector momentarily aligned with the velocity vector of the lizard, leading to a minimum in the centripetal acceleration curve. We used this centripetal acceleration minima in each glide track to mark the end of takeoff. *Mid-glide* followed takeoff as the lizard proceeded towards the eventual landing tree. The mid-glide phase usually consisted of the highest overall glide speed and a continuously shallowing

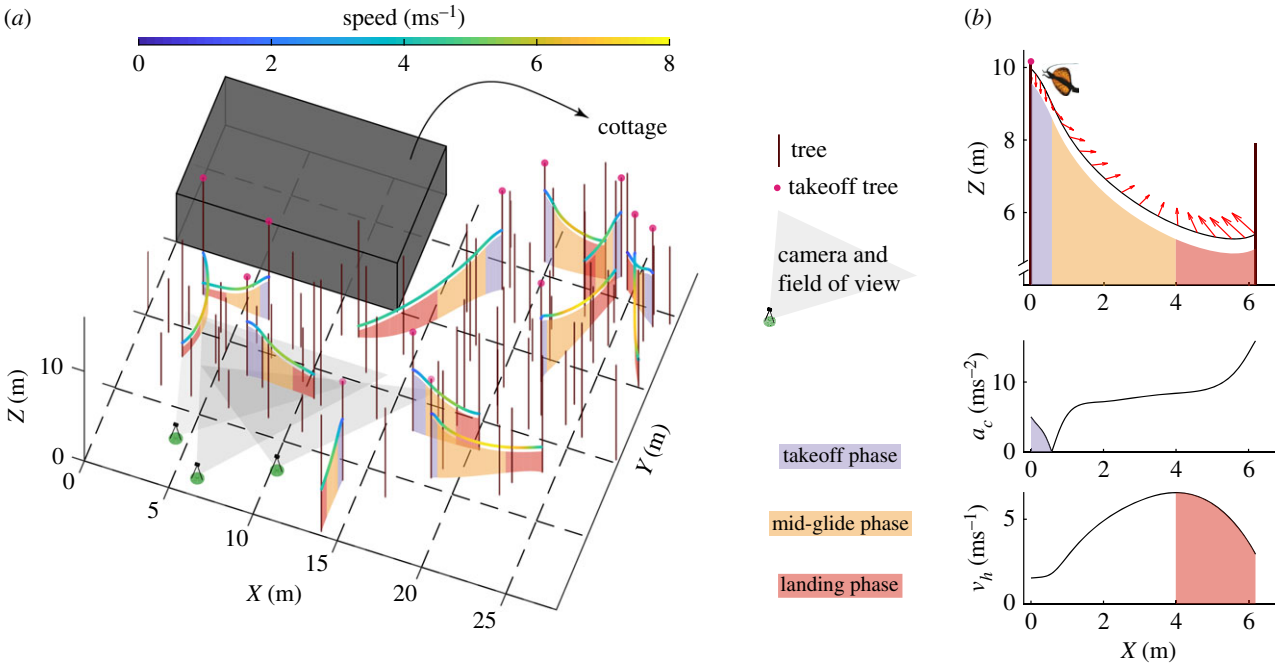

Figure 1. A scaled illustration of part of the field site, trajectories and glide phases. (*a*) An overview of part of the field site showing the distribution of trees and the trajectories of 11 out of 26 glides along with a sample camera array and a schematic of the field site cottage. Each glide is colour coded based on the speed of the lizard and divided into takeoff, mid-glide and landing phases. (*b*) Panel shows the side profile of a representative glide along with the behaviour and use of the kinematic parameters to divide each glide into takeoff, mid-glide and landing phases. The red arrows show the acceleration vectors in the *X*–*Z* plane at various instants of time along the glide path, transitioning from an almost vertically downwards (takeoff) to nearly horizontal in the forward direction (mid-glide) to vertically backwards for landing. The first minima in the centripetal acceleration (a_c) curve corresponds to the end of the takeoff phase where the acceleration vector aligns with the velocity vector. The landing phase begins with deceleration in horizontal speed (v_h). The part of the glide between takeoff and landing forms the mid-glide phase.

instantaneous glide angle. The end of the mid-glide phase was marked by the instant at which the lizard began to decelerate in the horizontal plane. *Landing* began with a decrease in horizontal speed and ended when the lizard reached the target tree. During landing, lizards continuously increased their body pitch and just before contact moved their forelimbs forward, their head back relative to their spine, and collapsed their wings.

(ii) Environmental effects—obstacles

The surrounding trees along the glide path were analysed as obstacles to locomotion. To simplify analysis and modelling, the tree with the smallest orthogonal distance (d_y) from a straight path between the takeoff and landing tree was defined as the obstacle for that glide. The obstacle was quantified by defining the absolute angle (γ) subtended by the obstacle tree on the takeoff tree in the horizontal plane as shown in figure 2*c*. The effect of the obstacle on the lizard's trajectory was quantified via takeoff direction (β) and the lateral acceleration (a_y) while passing the obstacle (a_{yO}), each calculated in the horizontal plane. Furthermore, we modelled the lizard as a simple fixed-wing glider to calculate the roll angle (equation (2.1)) required to generate the observed a_{yO} and thus infer losses in the aerodynamic lift force due to obstacles (figure 2*d*):

$$\text{roll angle} = \tan^{-1}\left(\frac{a_{yO}}{a_{zO}+9.81}\right), \tag{2.1}$$

where at the instant of passing the obstacle, a_{yO} is the observed lateral acceleration and $(a_{zO}+9.81)$ is the upward acceleration after accounting for body weight.

Lastly, to understand the influence of γ on landing tree choice, we simulated a forest with a tree distribution representative of the field site and calculated γ's for all possible combinations of takeoff and landing trees having a glide distance of less than 12 m. We then compared the recorded γ with the median of the simulated γ distribution for the observed glide distances to check for landing tree preferences in flying lizards.

(c) Visual landing control

We used the RREV model, also known as the tau (τ) strategy, to predict the initiation of a landing response during the glide [19,20]. This model suggests a critical value of the ratio of retinal expansion velocity (Ω) to the retinal size (α) of the landing tree where lizards initiate a deceleration response. The required quantities were calculated as follows [20]:

$$\text{RREV} = \frac{\Omega}{\alpha} = \frac{1}{\tau} \tag{2.2}$$

$$\alpha = 2\sin^{-1}\left(\frac{r}{d}\right) \tag{2.3}$$

$$\text{and} \quad \Omega = \frac{\mathrm{d}\alpha}{\mathrm{d}t} = \frac{-2v_h(r/d^2)}{\sqrt{1-(r/d)^2}}, \tag{2.4}$$

where $r = 0.10$ m (assumed radius of the landing tree), d is the distance of the lizard from the landing tree in the horizontal plane and v_h is the horizontal speed (figure 2*b*).

We implemented the model by aligning all glides greater than 2 m to begin their landing phase at $t = 0$ s, with $t > 0$ s corresponding to further into the landing phase. Glides less than 2 m ($n = 2$) matched the average tree spacing in the field site and due to their proximity may not require a landing trigger. The critical RREV value was calculated as the minima in the coefficient of variation (CV) of RREV values between −0.5 and 0.1 s across all glides.

(d) Steering model

We used an obstacle-avoidance steering model to understand how lizards adjusted their in-flight trajectory (heading direction, $\emptyset$, figure 2*c*) to reach the landing tree. This steering model [17]

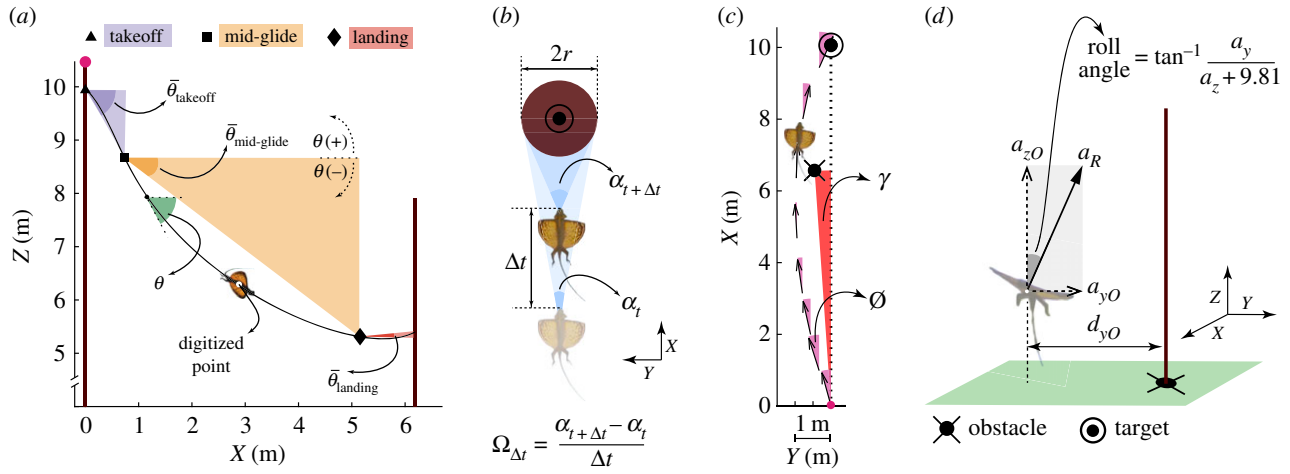

Figure 2. An illustration of the calculated glide parameters. (*a*) Calculation of the average takeoff ($\bar{\theta}_{takeoff}$), mid-glide ($\bar{\theta}_{mid-glide}$) and landing ($\bar{\theta}_{landing}$) angle. The instantaneous glide angle (θ) was used to calculate the shallowing rate of the mid-glide phase. (*b*) Overhead view (*X*–*Y* plane) of lizard approaching the target tree of radius '*r*' at two instants of time separated by Δt. The retinal size of the target changes from α_t to $\alpha_{t+\Delta t}$ such that the retinal expansion velocity is $\Omega_{\Delta t}$ at time instant $(t + \Delta t)$. (*c*) Overhead view (*X*–*Y* plane) showing the calculation of obstacle angle (γ) and the instantaneous heading angle (ϕ). (*d*) Front view (*Y*–*Z* plane) of the lizard at the instant of crossing the obstacle, showing the calculation of the modelled roll angle and the orthogonal distance (d_{y0}) from the obstacle tree. (Online version in colour.)

characterized the goal (landing tree) as an attractor and obstacle(s) as repellers of heading acceleration, modulated by the distance to the goal and obstacle(s). A linear combination of the attractor and all the repellers produced a final heading acceleration function for the track. We modelled the glide tracks based on the simplest obstacle-avoidance case with one obstacle for each glide track (obstacle-aware model, equation (2.5)).

$$\ddot{\emptyset}_{obstacle} = -b\dot{\emptyset} - k_g(\emptyset - \varphi_g)(e^{-c_1 d_g} + c_2) + k_o(\emptyset - \varphi_o)(e^{-c_3|\emptyset-\varphi_o|})(e^{-c_4 d_o}), \quad (2.5)$$

where at any instant of time in the horizontal plane: $\emptyset$ is the lizard's heading direction, φ_g and φ_o are the angle subtended by the landing tree (goal) and the obstacle on the lizard's position, d_g and d_o are the lizard's distance from the goal and the obstacle, and b, k_g, k_o and c_{1-4} are the tuning parameters.

By removing the obstacle term, we obtained the no-obstacle model:

$$\ddot{\emptyset}_{no\ obstacle} = -b\dot{\emptyset} - k_g(\emptyset - \varphi_g)(e^{-c_1 d_g} + c_2). \quad (2.6)$$

To test the performance of each of these models, the observed heading direction data were fit to equations (2.5) and (2.6) using the *fitnlm* MATLAB function; the relative goodness of fit of the models were compared using the Akaike information criterion corrected for small sample size (AICc).

(e) Statistical analysis

Linear relationships between glide and kinematic variables were tested using a least square regression (LSR) model performed with the *fitlm* function in MATLAB.

3. Results

A total of 33 glides were digitized (26 male and 7 female glides), out of which only 25 male glides were used for analysis; one was not considered because the lizard flew past the apparent target tree to land on a nearby tree. These 25 male glides excluded any known repeat glides from the same individual. Nevertheless, the local population density of approximately 4.7 lizards per 1000 m^2 (i.e. approx. 33 lizards at the recording site) makes it possible but not certain that some repeated sampling occurred; population exchange between the recording site and surrounding jungle preserve may have prevented even limited resampling. The seven female glides were excluded because females might be at different stages of their reproductive cycle during the mating season, influencing their gliding behaviour. Overall, male recorded glides varied in distance from 2 m to 10 m, with maximum glide speeds between 3.6 and 7.9 ms^{-1} and glide durations of 0.8–2.1 s.

(a) Takeoff phase

Lizards jumped from a height of 7.40 ± 1.91 m (mean ± s.d., $n = 25$) above ground level, independent of the glide distance (LSR, $p = 0.20$, figure 3*a*). In most cases, they did not take off directly towards the target tree, i.e. the takeoff direction (β) was not equal to 0°; β had an absolute value of 10.07 ± 9.46° and a maximum of 40.88°. Lizards directed their jumps farther away from obstacles more in line with the target tree (LSR, $R^2 = 0.22$, $p = 0.01$; figure 3*b*) and had higher lateral accelerations (a_{yO}) of 1.74 ± 1.63 ms^{-2} (LSR, $R^2 = 0.39$, $p < 0.001$) while passing the obstacle to reorient their glide towards the landing tree (figure 3*b*). The maximum a_{yO} observed was 6.34 ms^{-2} for a β of 40.88° and a γ of 5.69°. Average takeoff angles ($\bar{\theta}_{takeoff}$) ranged from −63.90° to −30.78°; steeper $\bar{\theta}_{takeoff}$ was associated with longer glide distances (LSR, $R^2 = 0.16$, $p = 0.03$; figure 3*c*) and higher maximum glide speeds (LSR, $R^2 = 0.58$, $p < 0.001$). On average, the takeoff phase lasted for 0.38 ± 0.06 s, independent of the glide distance (LSR, $p = 0.64$). Overall, lizards tuned their takeoff angle and direction with respect to the obstacle and landing tree position but maintained similar takeoff durations across glide distances.

(b) Mid-glide phase

Longer glides had marginally shallower mid-glide angles ($\bar{\theta}_{mid-glide}$) (LSR, $R^2 = 0.15$, $p = 0.03$); however, the average shallowing rate through mid-glide was 54.15 ± 14.29°s^{-1} and did not vary with glide distance (LSR, $p = 0.11$; figure 4*c*). Thus, shallower and longer glides were achieved by extending the mid-glide duration, a quantity strongly associated

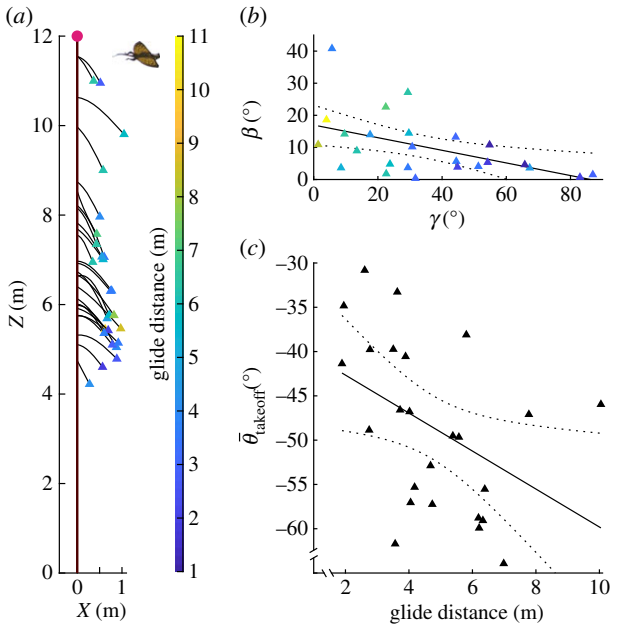

Figure 3. Takeoff phase. (*a*) Side view (*X*–*Z* plane) of takeoff phase for all 26 glides, showing variation in takeoff height and average takeoff angle ($\bar{\theta}_{takeoff}$). The end of each takeoff phase is marked by a colour coded triangle denoting the corresponding glide distance. (*b*) Inverse correlation between the takeoff direction (β) and the obstacle angle (γ), showing that lizards direct their jump farther away from obstacles closer to a straight path between the takeoff and landing tree. (*c*) Correlation between the average takeoff angle and glide distance indicating steeper dives for longer glide distances. (Online version in colour.)

with the final glide distance (LSR, $R^2 = 0.87$, $p < 0.001$). Interestingly, the average glide angle from the initiation of landing (from the RREV cue, see Results section on Visual landing control) to the end of the mid-glide phase was correlated with the total glide distance (LSR, $R^2 = 0.71$, $p < 0.001$). Obstacle position (angle γ) had no significant effect on the average mid-glide angle (LSR, $p = 0.12$) but corresponded to a marginally lower average shallowing rate (LSR, $R^2 = 0.13$, $p = 0.04$). The roll angle model further emphasized the weak obstacle effects on the mid-glide phase kinematics. Across all glides, we calculated a maximum roll angle of 21.08° from a recording with a γ of 1.38°, corresponding to a loss of 6.69% in the modelled lift force (figure 4*b*).

(c) Landing phase

With increasing glide distance, lizards entered the landing phase at higher horizontal speeds (LSR, $R^2 = 0.73$, $p < 0.001$) and had longer landing durations (LSR, $R^2 = 0.41$, $p < 0.001$). Furthermore, longer glides were associated with shallower landing angles ($\bar{\theta}_{landing}$) (LSR, $R^2 = 0.52$, $p < 0.001$) and higher maximum deceleration in the horizontal plane (LSR, $R^2 = 0.26$, $p < 0.01$) (figure 5*b*). The braking manoeuvre culminated in touchdown speeds of 0.83–5.74 ms^{-1}, approximately 1 to approximately 9 m (median height of 3.77 m) above the ground. The touchdown speed was slightly higher for longer glides (LSR, $R^2 = 0.20$, $p = 0.01$) but independent of the average landing angle (LSR, $p = 0.20$) and the maximum horizontal deceleration achieved (LSR, $p = 0.98$). Overall, with an increase in glide distance, lizards had extended landing durations and shallower landing angles with variable touchdown speeds.

(d) Effect of obstacles

Longer glides are expected to have smaller obstacle angles (γ) due to the distribution of trees at the field site (see Methods, γ with glide distance simulation) (figure 6*c*). However, the observed γ were significantly larger than that predicted by the simulation (Wilcoxon signed-rank test, $p < 0.001$; figure 6*c*). Additionally, smaller γ's corresponded to lizards performing high a_{yO} manoeuvres (LSR, $R^2 = 0.47$, $p < 0.001$) when passing the obstacle while maintaining a minimum lateral distance (d_{yO}) of 0.5 m from it.

(e) Visual navigation

The obstacle-aware (equation (2.5)) and no-obstacle (equation (2.6)) steering models were fitted to the observed heading data (see Methods; also figure 7). The best fit for both models was obtained with a response lag of 67 ms, with the obstacle-aware model (nonlinear LSR, $R^2 = 0.60$, $F_{7,1889} = 402$, $p < 0.001$) performing better than the no-obstacle model (nonlinear LSR, $R^2 = 0.57$, $\Delta AICc = 101.12$, $F_{4,1892} = 641$, $p < 0.001$).

(f) Visual landing control

Lizards initiated their landing response at a mean RREV of approximately 1.39 s^{-1} ($n = 23$) observed at 280 ms before the start of the landing phase, as shown in figure 8*a*. During the landing phase, we found that τ (inverse of RREV value) varied uniformly with time (figure 8*b*), i.e. $\dot{\tau}$ was held constant with a value of -0.84 ± 0.08 ($n = 23$; LSR, mean $R^2 \sim 1.00$, $p < 0.001$; Pearson correlation coefficient, mean $r \sim -1.00$, $p < 0.001$) indicating a 'controlled-collision' approach undertaken by lizards to land [18,26].

4. Discussion

Our study examined behaviourally motivated, complete glides of male flying lizards over varying degrees of spatial complexities and glide distances. In this context, we found that flying lizards employ a visually guided path planning strategy to traverse their aerially cluttered natural environment. Specifically, lizards performed non-equilibrium glides along paths with relatively less surrounding clutter and adjusted their takeoff to accommodate for topography and the desired glide distance. Furthermore, their glide trajectories were consistent with vision-based control models for navigation, obstacle-avoidance and landing.

(a) Equilibrium versus non-equilibrium gliding

To perform an equilibrium glide, the animal must hold a static gliding pose for an extended duration along a straight path to balance the gravitational and aerodynamic forces, yielding a constant glide velocity [4,27]. Equilibrium gliding as a common mode of glide execution has been described in colugos [10] and gliding lizards [12] but appears to be absent in flying snakes [14] and squirrels [13], questioning the prevalence and feasible conditions of equilibrium gliding in nature. In *Draco*, McGuire & Dudley [12] found that 48% of recorded glides (with complete speed profile) reached equilibrium. However, the individuals were coaxed to glide between a fixed takeoff and landing pole, placed 9.3 m apart, with no other destination options (few landings were on the ground), and no obstacles.

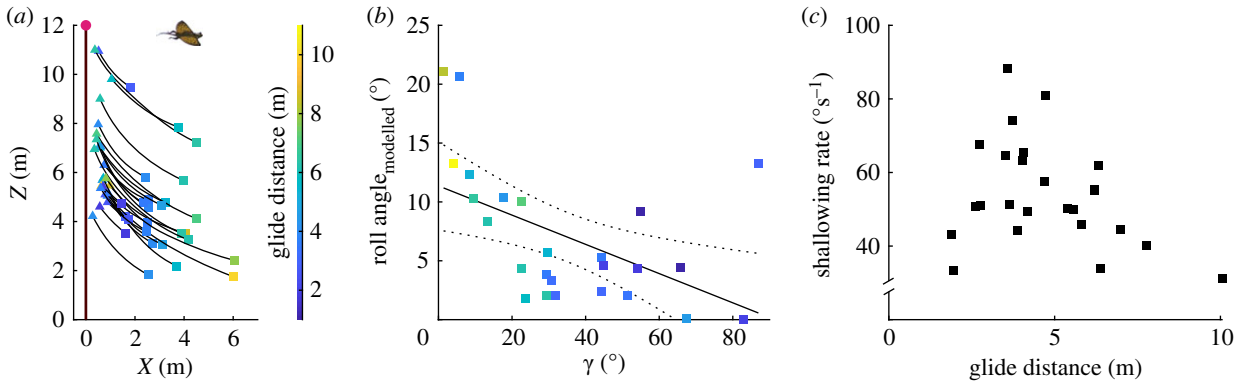

Figure 4. Mid-glide phase. (*a*) Side view (*X*–*Z* plane) of mid-glide phase for all 26 glides, colour coded with respect to their glide distance. Longer glides have extended mid-glide phases. (*b*) Model results simulating the roll angles for a fixed-wing glider to generate observed a_{y0} while passing the obstacle tree. The model shows a maximum roll angle of approximately 21° for an obstacle almost in line with the landing tree. (*c*) A scatter plot showing the mid-glide shallowing rate to be invariant across all glides. (Online version in colour.)

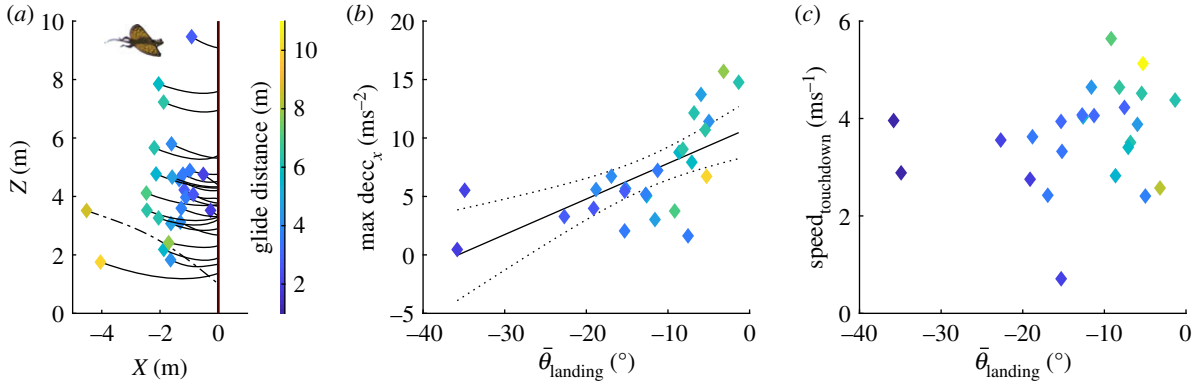

Figure 5. Landing phase. (*a*) Side view (*X*–*Z* plane) of landing phase for all 26 glides, colour coded with respect to their glide distance. The dashed line shows an aborted landing, not following the stereotypical shallowing curve of other landing trajectories. (*b*) As expected, shallower average landing angles ($\bar{\theta}_{landing}$) correspond to higher maximum deceleration in the forward direction. (*c*) The touchdown speed is independent of $\bar{\theta}_{landing}$, showing a range of impact speeds employed by lizards. (Online version in colour.)

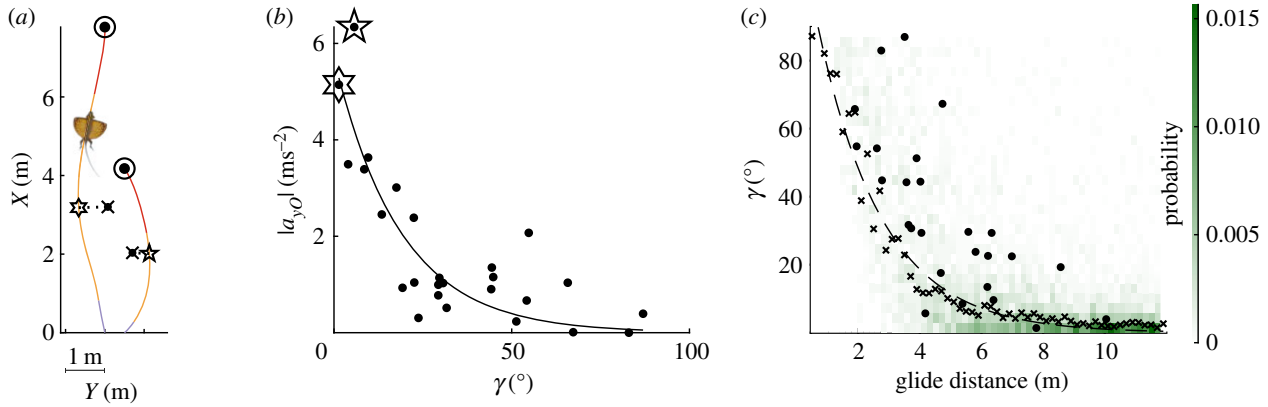

Figure 6. Obstacle-avoidance and path choice. (*a*) Overhead view of two representative glides portraying obstacle-avoidance, colour coded to show the glide phases. Both glides show the lizard taking off in a direction away from the obstacle. The location of lateral acceleration (a_{y0}) calculation is marked by ☆ and ☆ for each glide. (*b*) Magnitude of lateral acceleration (|a_{y0}|) calculated while passing the obstacle decreases exponentially with an increase in obstacle angle (γ). (*c*) Probability density map of simulation of obstacle angles varying with glide distances in the topography of our field site. The dashed line shows that the median of simulated obstacle angles, marked by '**x**', decreases exponentially as a function of glide distance. The observed γ-values for our recorded glides, marked by '•', were higher for 22 out of 25 glides compared to the simulated γ of similar glide distance. (Online version in colour.)

We hypothesized that most natural habitats provide little opportunity for animals to glide the distances required to achieve equilibrium gliding without adjusting their glide path or speed to negotiate obstacles. This implies that non-equilibrium gliding is the predominant mode of glide execution for *Draco* in their natural habitat. Our results support this hypothesis, as none of our quantified glides reached equilibrium. Furthermore, the highest probability for lizards to achieve equilibrium gliding is in the mid-glide phase where they are not accelerating or braking as observed in takeoff

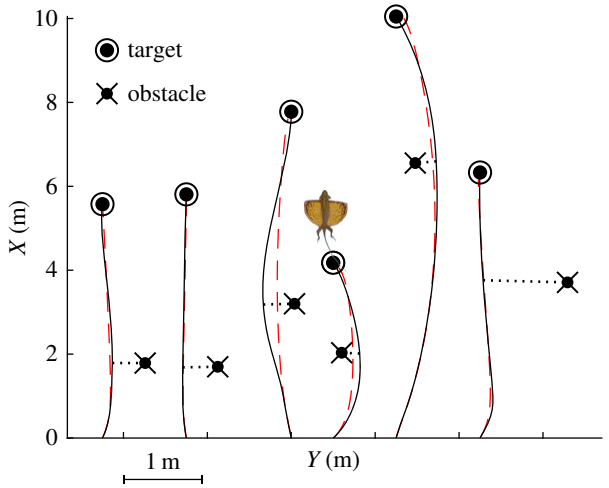

Figure 7. Vision-based obstacle-avoidance model. Overhead view (*X*–*Y* plane) of 6 out of 25 glides of varying glide distances and obstacle positions showing the observed glide path (solid black line) along with the glide paths predicted by the obstacle-avoidance model (dashed red line). The model agreed with most glides, excluding a few with $\gamma < 20°$. (Online version in colour.)

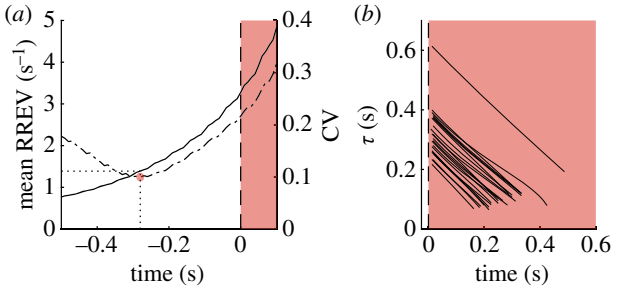

Figure 8. RREV model and the τ function. All glides were aligned to begin their landing phase at $t = 0$ s, with $t > 0$ s to be further into the landing phase. (*a*) The coefficient of variation (CV) reached a minimum at 280 ms before the start of the landing phase corresponding to a mean RREV value of 1.39 s^{-1}. (*b*) The τ value for each glide calculated as α/Ω reduced at a constant rate of 0.84 ± 0.08, suggesting a controlled-collision landing approach. (Online version in colour.)

and landing. However, we found that flying lizards in mid-glide shallowed their trajectory at a rate of $54.15 \pm 14.29°$ s^{-1}, much greater than rates observed in flying snakes [14,28] and sugar gliders [7]. Moreover, the average shallowing rate was independent of the glide distance (figure 4*c*), but was marginally lower for glides with obstacles more in line with the target tree (smaller γ's), suggesting that lizards exhibit steeper glide paths while performing in-flight lateral manoeuvres. To manoeuvre, the aerodynamic force vector is rotated about the roll axis of the body to cause lateral deviations, thus, reducing the upwardly directed lift force and resulting in a steeper glide path or lower shallowing rate. In our model for a fixed-wing glider generating identical lateral accelerations (a_{yO}) while passing the obstacle, the roll angles varied approximately between 0° and 21° (figure 4*b*) with a maximum loss in lift production of approximately 7%, further emphasizing the relationship between shallowing rate and the obstacle tree location. These results suggest that flying lizards actively manipulate body orientation and/or wing area to alter and direct aerodynamic forces while gliding, similar to mammalian gliders [7,8]. However, the absence of equilibrium gliding in our study does not show *Draco* to be incapable of attaining constant velocity glides in natural settings, just that lizards might choose not to use equilibrium gliding, or that opportunities to attain steady-state dynamics were rare or non-existent at our site. Our simulation of γ, the obstacle angle, as a function of glide distance in our field site yielded high probability of obstacle encounter for glide distances of 10 m or more (figure 6*c*), roughly the fixed glide distance tested by McGuire & Dudley. In comparison, the majority of our recorded glides were much shorter (median = 4.18 m). Nonetheless, it is also worth noting that McGuire & Dudley recorded glides in a two-dimensional (*X*–*Z*) plane using a single video camera, which would slightly limit the ability to detect lateral variations along the glide path, thus increasing the chances of incorrectly identifying equilibrium glides.

(b) Path planning *versus* reactive in-flight manoeuvres

Reaching the target tree in an aerially cluttered environment can be achieved by implementing a pre-defined collision-free path (path planning) and/or reactively altering the path as and when an obstacle is encountered (reactive manoeuvring). To manoeuvre, a glider must redirect the existing aerodynamic forces to generate centripetal acceleration, resulting in a decrease in upwardly directed force and an increase in gliding costs (energy). Thus, following the assertion of Caple *et al*. [29], we hypothesized that flying lizards would preferentially use a path planning strategy to minimize the energetic costs of negotiating obstacles, or alternatively, perform shorter obstacle-free glides to altogether avoid encountering these issues.

We quantified lizards performing glides of 2–10 m, with obstacle angles (γ) ranging between 1.4° and 87°. For a given glide distance, lizards jumped in a direction with less surrounding clutter than alternatives, suggesting that they opt for glide paths which will lead to relatively less loss of altitude due to in-flight manoeuvring (see Results; figure 6*c*). Furthermore, they modulated their takeoff to account for the expected glide distance and obstacles, using marginally steeper takeoff angles for longer glides and jumping farther away from obstacles directly in line with the target tree (figure 3*b*). Though the takeoff angle and direction varied, the takeoff duration was independent of glide distance and obstacle presence. Takeoff duration may instead be related to a morphological constraint of time taken for the complete wing and lappet deployment to generate lift. Nonetheless, the unique wing apparatus of *Draco* leads to a relatively streamlined pose immediately after jumping, allowing them to rapidly gain speed with their wings and appendages tucked close to their body. In a cluttered environment, the rapid gain in speed might facilitate manoeuvring earlier in the glide compared to mammalian gliders that take an abducted body pose [6] to extend their wing surface, leading to increased overall drag.

Together, these results show that flying lizards pre-select their target tree based on the topography and accordingly adjust their takeoff phase to successfully execute a glide. However, as glide distance increases, planning a collision-free path through a cluttered environment becomes increasingly less feasible, likely increasing the importance of reactive in-flight manoeuvres. This was indeed the case, with two glides with $\gamma < 10°$ and obstacles greater than 3 m from the takeoff tree exhibiting reactive in-flight manoeuvres (figure 6*a*, glide on the left), indicating that both strategies contribute towards lizards navigating their environment. Overall, we provide

evidence for a path planning strategy used by flying lizards in a cluttered environment, with the increased possibility of reactive in-flight manoeuvres for smaller γ and longer glide distances.

(c) Visual navigation

Vision is believed to be the primary sensory modality used by most gliders for flight control [4]. Canopy ants *Cephalotes atratus* use brightness cues to orient themselves during a fall and to land on the tree [30], highlighting the role of vision in glide navigation and control. The gliding lizard *Draco sumatranus* adjust their position on the tree relative to the sun to make their dewlap easily visible to conspecifics during social interactions [31], supporting that vision is likely to be the primary sensory input used by *Draco* to gather information from their surroundings. However, testing the contribution of vision to navigation and/or path control can be extremely challenging, requiring manipulating the visual field of the animal in real time during flight [4]. Instead, here we provide indirect support by fitting pre-existing visual control models to heading direction (navigation) and landing kinematics (control).

We hypothesized that flying lizards navigate towards the landing tree by using an obstacle-avoidance steering model [17]. Even in cases where no obstacles were present, the lizards took off at an angle offset from a straight line between takeoff and landing trees ($\beta > 0°$), thus requiring some in-flight lateral manoeuvres. We saw good agreement between the heading direction of lizards and that predicted by the model after incorporating a time shift of 67 ms, implying a visuomotor delay. The time delay was comparable to the minimum retinal integration time of approximately 67 ms reported in *Anolis* lizards (flicker fusion frequency in the 15–30 Hz range) [32] but short compared to visuomotor delays in other flying species [3], suggesting that our observations include feedforward and feedback components. Next, we removed the obstacle component from the model and saw reduced predictive power (ΔAICc = 101.12, see Results), indicating that flying lizards indeed consider obstacles while gliding. Overall, the model suggests that flying lizards adjust their heading direction to align in the direction of their target while maximizing the bearing angle to the obstacle. Nonetheless, we did observe reactive in-flight manoeuvres which were poorly replicated by the model. These manoeuvres corresponded to obstacles farther away from the takeoff tree (greater than 3 m), potentially making them less conspicuous at the time of takeoff (figure 7).

(d) Visual landing control

To land, we hypothesized that flying lizards use a RREV model, also known as the τ strategy. The τ strategy has been used to describe the onset of landing in flies [19,20] and pigeons [18]. In the wild, plummeting gannets were shown to use a τ strategy to trigger streamlining just before entering the water surface to forage [33]. Hence, in vision-based animals, the τ strategy could provide a simple way of integrating surrounding information to control the timing of certain locomotory behaviours. For *Draco*, the locomotory behaviour is the initiation of the body pitch-up landing manoeuvre to decelerate. Our data fit exceptionally well with the RREV model and show 280 ms prior to the start of the landing phase as the decision point to initiate a body pitch-up braking manoeuvre. Interestingly, for glides less than 3 m, the 280 ms response time corresponds to the start of the mid-glide phase, i.e. in shorter glides (less than 3 m), lizards prepare to land immediately after the takeoff phase, essentially using the mid-glide to initiate braking.

By pitching up to land, flying lizards present more frontal area in the direction of motion, dissipating part of the accumulated kinetic energy as drag. However, the magnitude of deceleration is limited by the wing area; in other words, long glides with higher speeds require extended landing durations to reach a safe touchdown speed and thus, lizards should enter the landing phase farther away from the target tree. As expected, with an increase in glide distance and speed, lizards had longer landing durations corresponding to shallower landing angles and higher maximum deceleration. Interestingly, the speed at touchdown was variable (0.83–5.74 ms^{-1}; figure 5*c*) and lizards maintained a constant $\dot{\tau}$ of 0.85 ± 0.08 during landing, suggesting that they approach the target tree using a 'controlled-collision procedure' [18]. Here, flying lizards gradually increase their braking as the target gets closer, culminating in a non-zero touchdown velocity. For unpowered flight, such a strategy might allow maintaining lift during deceleration to alleviate the risk of stalling, or, facilitate evasive manoeuvres if the landing site is unfavourable upon closer inspection (e.g. predator and/or a territorial male). We did record an aborted landing in one of our glides where the lizard turned away from the initial target tree to land instead on a nearby tree (figure 5*a*).

Finally, pitching up also increases the upward force, potentially allowing lizards to regain some lost altitude by performing a terminal upswing, as noted previously in flying lizards [12] and squirrels [13]. From the lowest point in the glide trajectory, we saw marginally increasing gain in altitude of up to approximately 4.5% of the total height lost, with a maximum gain of 0.19 m for a glide distance of 6.21 m. This small gain increased with glide distance, suggesting that the terminal upswing is likely a feature of longer glides but still represents only a small fraction of the total height lost.

5. Conclusion

By integrating aspects of the environment, behaviour and the biomechanical capabilities of the glider, we show flying lizards using a visually guided path planning strategy to perform collision-free flight in a naturally cluttered habitat. Furthermore, our study provides insight into how gliders use and process visual information from the environment, beginning from pre-selecting the target tree, adjusting their heading direction, to initiating and controlling their braking to land. Together, these unique set of results reveal previously unknown capabilities in gliding animals and demonstrate the importance of field studies in gaining a more comprehensive understanding of ecologically relevant locomotory behaviours.

Ethics. Data collection was based on video recording the glides from a distance along with behavioural observations and did not involve handling or interacting with the animals. This minimized any disturbance that might influence the behaviour of the lizard and did not require any handling permits for data collection. The ARRS campus is privately owned and does not fall within a protected area [19], exempting us from requiring government permits. The study was conducted with permission from the local ARRS authorities and as per UNC Institutional Animal Care and Use Committee guidelines.

Data accessibility. The kinematic data and analysis routines that produced the results presented in this project are from the Dryad Digital Repository: https://doi.org/10.5061/dryad.70rxwdbt6 [34].

Authors' contributions. P.C.K. conceived of the study, performed field data collection, data analysis, data interpretation and manuscript authorship. T.L.H. performed data analysis, data interpretation and manuscript authorship.

Competing interests. We declare we have no competing interests

Funding. This project was funded by NSF IOS-1253276 to T.L.H.

Acknowledgements. We wish to thank two anonymous referees for their comments as well as Jonathan Rader and other members of the Hedrick lab for their feedback on this project. We would also like to thank Dr. Sanjay P. Sane, Deepak CK, Dhiraj Bhaisare, Ajay Giri and the local staff at ARRS for hosting and assisting with field data collection.

References

1. Parker SE, McBrayer LD. 2016 The effects of multiple obstacles on the locomotor behavior and performance of a terrestrial lizard. *J. Exp. Biol.* **219**, 1004–1013. (doi:10.1242/jeb.120451)
2. Jayaram K, Mongeau JM, Mohapatra A, Birkmeyer P, Fearing RS, Full RJ. 2018 Transition by head-on collision: mechanically mediated manoeuvres in cockroaches and small robots. *J. R. Soc. Interface* **15**, 20170664. (doi:10.1098/rsif.2017.0664)
3. Lin HT, Ros IG, Biewener AA. 2014 Through the eyes of a bird: modelling visually guided obstacle flight. *J. R. Soc. Interface* **11**, 20140239. (doi:10.1098/rsif.2014.0239)
4. Socha JJ, Jafari F, Munk Y, Byrnes G. 2015 How animals glide: from trajectory to morphology. *Can. J. Zool.* **93**, 901–924. (doi:10.1139/cjz-2014-0013)
5. Essner RL. 2002 Three-dimensional launch kinematics in leaping, parachuting and gliding squirrels. *J. Exp. Biol.* **205**, 2469–2477.
6. Paskins KE, Bowyer A, Megill WM, Scheibe JS. 2007 Take-off and landing forces and the evolution of controlled gliding in northern flying squirrels *Glaucomys sabrinus*. *J. Exp. Biol.* **210**, 1413–1423. (doi:10.1242/jeb.02747)
7. Bishop KL. 2007 Aerodynamic force generation, performance and control of body orientation during gliding in sugar gliders (*Petaurus breviceps*). *J. Exp. Biol.* **210**, 2593–2606. (doi:10.1242/jeb.002071)
8. Bishop KL. 2006 The relationship between 3-D kinematics and gliding performance in the southern flying squirrel, *Glaucomys volans*. *J. Exp. Biol.* **209**, 689–701. (doi:10.1242/jeb.02062)
9. Bishop KL, Brim-Deforest W. 2008 Kinematics of turning maneuvers in the southern flying squirrel, *Glaucomys volans*. *J. Exp. Zool. Part A Ecol. Genet. Physiol.* **309**, 225–242. (doi:10.1002/jez.447)
10. Byrnes G, Lim NTL, Spence AJ. 2008 Take-off and landing kinetics of a free-ranging gliding mammal, the Malayan colugo (*Galeopterus variegatus*). *Proc. R. Soc. B* **275**, 1007–1013. (doi:10.1098/rspb.2007.1684)
11. Byrnes G, Libby T, Lim NTL, Spence AJ. 2011 Gliding saves time but not energy in Malayan colugos. *J. Exp. Biol.* **214**, 2690–2696. (doi:10.1242/jeb.052993)
12. McGuire JA, Dudley R. 2005 The cost of living large: comparative gliding performance in flying lizards (Agamidae: *Draco*). *Am. Nat.* **166**, 93–106. (doi:10.1086/430725)
13. Bahlman JW, Swartz SM, Riskin DK, Breuer KS. 2013 Glide performance and aerodynamics of non-equilibrium glides in northern flying squirrels (*Glaucomys sabrinus*). *J. R. Soc. Interface* **10**, 20120794. (doi:10.1098/rsif.2012.0794)
14. Socha JJ, Miklasz K, Jafari F, Vlachos PP. 2010 Non-equilibrium trajectory dynamics and the kinematics of gliding in a flying snake. *Bioinspiration Biomim.* **5**, 045002. (doi:10.1088/1748-3182/5/4/045002)
15. Suzuki K, Asari Y, Yanagawa H. 2012 Gliding locomotion of Siberian flying squirrels in low-canopy forests: the role of energy-inefficient short-distance glides. *Acta Theriol. (Warsz).* **57**, 131–135. (doi:10.1007/s13364-011-0060-y)
16. Suzuki KK, Yanagawa H. 2019 Gliding patterns of Siberian flying squirrels in relation to forest structure. *iForest* **12**, 114–117. (doi:10.3832/ifor2954-011)
17. Fajen BR, Warren WH. 2003 Behavioral dynamics of steering, obstacle avoidance, and route selection. *J. Exp. Psychol. Hum. Percept. Perform.* **29**, 343–362. (doi:10.1037/0096-1523.29.2.343)
18. Lee DN, Davies MNO, Green PR, Van Der Weel FR(Ruud). 1993 Visual control of velocity of approach by pigeons when landing. *J. Exp. Biol.* **180**, 85–104.
19. Wagner H. 1982 Flow-field variables trigger landing in flies. *Nature* **297**, 147–148. (doi:10.1038/297147a0)
20. Van Breugel F, Dickinson MH. 2012 The visual control of landing and obstacle avoidance in the fruit fly *Drosophila melanogaster*. *J. Exp. Biol.* **215**, 1783–1798. (doi:10.1242/jeb.066498)
21. Khandelwal P., Shankar C., Hedrick T. 2018 Take-off biomechanics in gliding lizards. *Soc. Integr. Comp. Biol.* **1**, 38–41. See http://www.sicb.org/meetings/2018/schedule/abstractdetails.php?id=985.
22. Sreekar R, Purushotham CB, Saini K, Rao SN, Pelletier S, Chaplod S. 2013 Photographic capture-recapture sampling for assessing populations of the Indian gliding lizard *Draco dussumieri*. *PLoS ONE* **8**, e55935. (doi:10.1371/journal.pone.0055935)
23. Srinivasulu C, Srinivasulu B, Vijayakumar SP, Ramesh M, Ganesan SR, Madala M, Sreekar R. 2013 *Draco dussumieri*. See http://dx.doi.org/10.2305/IUCN.UK.2013-1.RLTS.T172625A1354495.en.
24. McGuire JA, Dudley R. 2011 The biology of gliding in flying lizards (genus *Draco*) and their fossil and extant analogs. *Integr. Comp. Biol.* **51**, 983–990. (doi:10.1093/icb/icr090)
25. Colbert EH. 1967 Adaptations for gliding in the lizard *Draco*. *Am. Mus. Novit.* **2283**, 1–20.
26. Lee DN, Reddish PE, Rand DT. 1991 Aerial docking by hummingbirds. *Naturwissenschaften* **78**, 526–527. (doi:10.1007/BF01131406)
27. Norberg UM. 1985 Evolution of vertebrate flight: an aerodynamic model for the transition from gliding to active flight. *Am. Nat.* **126**, 303–327. (doi:10.1086/284419)
28. Socha JJ, O'Dempsey T, LaBarbera M. 2005 A 3-D kinematic analysis of gliding in a flying snake, *Chrysopelea paradisi*. *J. Exp. Biol.* **208**, 1817–1833. (doi:10.1242/jeb.01579)
29. Caple G, Balda RP, Willis WR. 1983 The physics of leaping animals and the evolution of preflight. *Am. Nat.* **121**, 455–476. (doi:10.1086/284076)
30. Yanoviak SP, Dudley R. 2006 The role of visual cues in directed aerial descent of *Cephalotes atratus* workers (Hymenoptera: Formicidae). *J. Exp. Biol.* **209**, 1777–1783. (doi:10.1242/jeb.02170)
31. Klomp DA, Stuart-Fox D, Das I, Ord TJ. 2017 Gliding lizards use the position of the sun to enhance social display. *Biol. Lett.* **13**, 20160979. (doi:10.1098/rsbl.2016.0979)
32. Pallus AC, Fleishman LJ, Castonguay PM. 2010 Modeling and measuring the visual detection of ecologically relevant motion by an Anolis lizard. *J. Comp. Physiol. A Neuroethol. Sens. Neural Behav. Physiol.* **196**, 1–13. (doi:10.1007/s00359-009-0487-7)
33. Lee DN, Reddish PE. 1981 Plummeting gannets: a paradigm of ecological optics. *Nature* **293**, 293–294. (doi:10.1038/293293a0)
34. Khandelwal PC, Hedrick TL. 2020 Data from: How biomechanics, path planning and sensing enable gliding flight in a natural environment. Dryad Digital Repository. (doi:10.5061/dryad.70rxwdbt6)